Journal of Solid State Chemistry 181 (2008) 2127–2132

Contents lists available at ScienceDirect

Journal of Solid State Chemistry

journal homepage: www.elsevier.com/locate/jssc

Hydrothermal synthesis of antimony oxychloride and oxide nanocrystals: $Sb_4O_5Cl_2$, $Sb_8O_{11}Cl_2$, and Sb_2O_3

Xiang Ying Chen, Hyun Sue Huh, Soon W. Lee *

Department of Chemistry (BK21), Sungkyunkwan University, Natural Science Campus, Suwon 440-746, Republic of Korea

ARTICLE INFO

Article history:
Received 10 November 2007
Received in revised form
24 January 2008
Accepted 29 April 2008
Available online 14 May 2008

Keywords:
Nanocrystals
Antimony oxychlorides and oxides
Senarmontite
Valentinite
Emission

ABSTRACT

We described herein a facile solution-phase route to three nanocrystals of antimony oxychlorides and oxides ($Sb_4O_5Cl_2$, $Sb_8O_{11}Cl_2$, and Sb_2O_3), whose morphologies and phases were varied with the pH value of a reaction mixture or composition of a mixed solvent. In particular, the solvent composition controlled the selective preparation of cubic Sb_2O_3 (senarmontite) and orthorhombic Sb_2O_3 (valentinite). Both cubic and orthorhombic Sb_2O_3 samples exhibited strong emission properties.

1. Introduction

Considerable attention has continually been paid to the synthesis of nanomaterials with controlled phases, sizes, and morphologies on which their characteristic properties strongly depend. Over a couple of the past decades, many research groups have devoted considerable efforts to preparing such nanomaterials [1,2].

Several nonstoichiometric antimony oxychlorides and oxides such as SbOCl, Sb_3O_4Cl, $Sb_4O_5Cl_2$, $Sb_8O_{11}Cl_2$, Sb_2O_3, Sb_2O_4, and Sb_2O_5 have been widely used in various industries. Sb_2O_3 typically has two polymorphs, cubic polymorph (senarmontite, stable phase) and orthorhombic polymorph (valentinite, metastable phase), and the orthorhombic polymorph can be transformed into the cubic one at 490–530 °C [3]. Senarmontite has long been used as an additive to enhance the flame retardancy of polymer resins, whereas valentinite has not due to its undesirable oxidization when exposed to air or sunlight [4]. Senarmontite was shown to act as a catalyst in combination with vanadium for the selective oxidation of *o*-xylene [5]. Valentinite is a major component of the Sb_2O_3–B_2O_3 binary glasses possessing nonlinear optical properties [6]. Besides senarmontite, some other antimony oxychlorides (SbOCl, $Sb_4O_5Cl_2$, $Sb_8O_{11}Cl_2$) also exhibit excellent flame retardancy when utilized alone or in combination with halogenated organic compounds [7].

Up to now, several 1-D Sb_2O_3 nanomaterials such as nanorods [8], nanowires [9], and nanobelts [10] have been prepared. On the other hand, antimony oxychloride nanomaterials are rare mainly due to their preparative difficulties. Nevertheless, a couple of nanostructured antimony oxychlorides were prepared previously. For example, Johnsson and co-workers prepared $Sb_8O_{11}Cl_2$ single crystals from Sb_2O_3 and $SbCl_3$ at 500 °C [11]. In addition, $Sb_4O_5Cl_2$ single crystals were recently synthesized in aqueous HCl solution [12]. However, there has been no report on the synthesis of nanometer-size $Sb_4O_5Cl_2$ and $Sb_8O_{11}Cl_2$.

In this study, we prepared antimony oxychloride and oxide nanocrystals by solution-phase methods. To our best knowledge, we are the first to report on the synthesis of $Sb_4O_5Cl_2$ nanoparticles and $Sb_8O_{11}Cl_2$ nanobelts and nanowires on a large scale. In particular, cubic and orthorhombic Sb_2O_3 could be prepared selectively by altering the solvent composition. Optical properties of the Sb_2O_3 samples were also examined at room temperature.

2. Experimental section

All chemicals were purchased, and all reactions were carried out in a 100 ml Teflon-lined stainless autoclave. The acidity (pH) of the reaction solution was adjusted by adding an appropriate amount of aqueous 6 M NaOH solution. Detailed reaction conditions were summarized in Table 1.

* Corresponding author. Fax: +82 31 290 7075.
E-mail address: swlee@chem.skku.ac.kr (S.W. Lee).

0022-4596/$ - see front matter © 2008 Elsevier Inc. All rights reserved.
doi:10.1016/j.jssc.2008.04.043

Table 1
Summary of reaction conditions

Product	Reactants	Mixed solvent (v/v: 1:1)	pH
$Sb_4O_5Cl_2$	$SbCl_3$	EG–H_2O EtOH–H_2O	1–2
$Sb_8O_{11}Cl_2$	$SbCl_3$+NaOH	EG–H_2O EtOH–H_2O	4–5
Sb_2O_3	$SbCl_3$+NaOH	EG–H_2O EtOH–H_2O	8–9

Notes: (1) In all cases, an initial amount of $SbCl_3$ is 2 mmol, and the total volume of a mixed solvent is 40 ml. (2) All the reactions were conducted at 120 °C for 12 h. (3) No NaOH is required in preparing $Sb_4O_5Cl_2$ because $SbCl_3$ hydrolyzes to give an acidic solution with pH = 1–2.

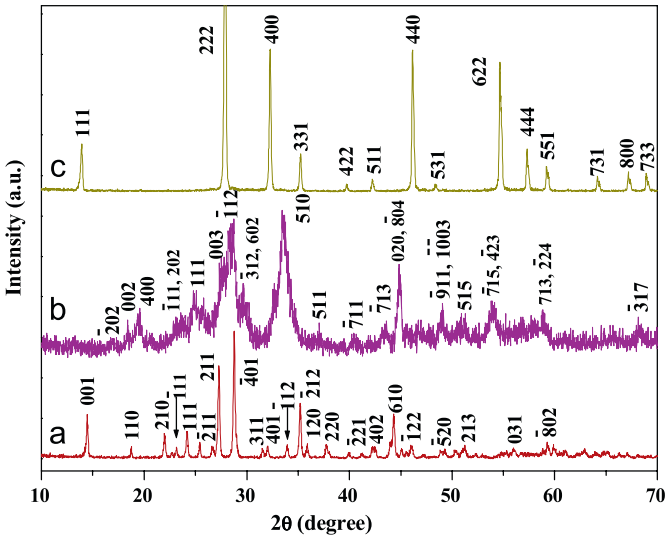

Fig. 1. XRPD patterns of the samples obtained in EG–H_2O (v/v, 1:1) at pH = 1–2 (a), 4–5 (b), and 8–9 (c).

2.1. A typical synthetic procedure for preparing cubic Sb_2O_3 in EG–H_2O

$SbCl_3$ (2 mmol) was dissolved in ethylene glycol (EG, 20 ml) under constant stirring to form a transparent solution, and then distilled H_2O (20 ml) was added to the solution to give lacteous colloids. The resulting mixture was stirred for 15 min, and the pH value was adjusted to 8–9 by adding 6 M NaOH(aq). The solution was further stirred for 20 min and transferred into a 100 ml Teflon-lined stainless autoclave, which was then sealed and kept at 120 °C. After 12 h, the resulting white product was filtered off, washed with distilled water (3 × 100 ml) and absolute ethanol (2 × 40 ml), and then dried under vacuum at 60 °C for 6 h.

2.2. Characterization

X-ray powder diffraction (XRPD) spectra were obtained on a Rigaku Max-2200 with Cu $K\alpha$ radiation. Transmission electron microscope (TEM) and high-resolution transmission electron microscope (HRTEM) images were taken with a JEOL 2100F unit operated at 200 kV at the Cooperative Center for Research Facilities (CCRF) in Sungkyunkwan University. Photoluminescence (PL) spectra were recorded with an AB2 spectrophotometer (Amico Bowmann).

3. Results and discussion

The phase, crystallinity, and purity of the samples, which were prepared in a mixed solvent at 120 °C for 12 h, were examined by XRPD. Fig. 1 shows the typical XRPD patterns of the samples obtained in EG–H_2O (v/v, 1:1) at three pH ranges. The reflection peaks in Fig. 1a (pH = 1–2) can be readily indexed as monoclinic $Sb_4O_5Cl_2$ (JCPDS card 30-0091). When the pH of the reaction mixture was increased to 4–5 by adding 6 M NaOH(aq), monoclinic $Sb_8O_{11}Cl_2$ (JCPDS card 77-1583) was produced (Fig. 1b). Furthermore, cubic Sb_2O_3 (Fig. 1c, JCPDS card 05-0534) was produced at pH = 8–9. No peaks assignable to $Sb_4O_5Cl_2$, $Sb_8O_{11}Cl_2$, or other phases of Sb_2O_3 appear in Fig. 1c, which strongly supports the formation of genuine cubic Sb_2O_3.

In order to investigate the effects of solvent composition on the identity of the products, we performed the reactions in another mixed solvent (EtOH–H_2O). At pH = 1–2 (Fig. 2a) and 4–5

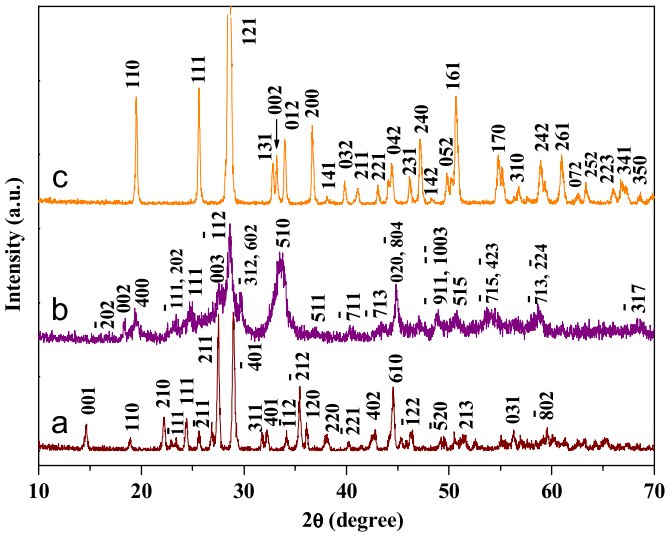

Fig. 2. XRPD patterns of the samples prepared in EtOH–H_2O (v/v, 1:1) at pH = 1–2 (a), 4–5 (b), and 8–9 (c).

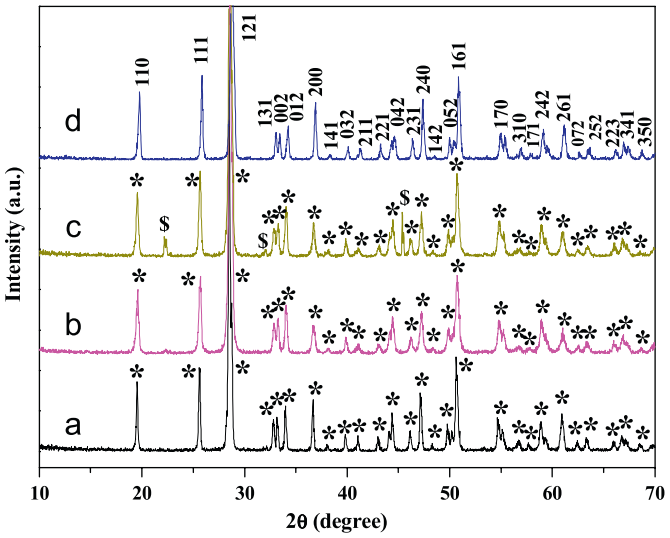

Fig. 3. XRPD patterns of the samples obtained at pH = 8–9 in mixed solvents (v/v, 1:1): (a) dmf–H_2O, (b) toluene–H_2O, (c) acetone–H_2O, and (d) en–H_2O. *Orthorhombic Sb_2O_3 (JCPDS 11-0689) and $ cubic Sb_2O_3 (JCPDS 72-1334).

(Fig. 2b), the products are identical with those prepared in EG–H_2O. However, orthorhombic Sb_2O_3 (JCPDS card 11-0689) was formed at pH = 8–9 in EtOH–H_2O (Fig. 2c), which contrasts with the fact that cubic Sb_2O_3 was formed in EG–H_2O in the same pH range (Fig. 1c).

From the XRPD patterns in Figs. 1 and 2, we can see that the acidity (pH) of a reaction mixture is critical to controllably preparing $Sb_4O_5Cl_2$, $Sb_8O_{11}Cl_2$, and Sb_2O_3. In addition, the solvent composition also appears to control the phase of Sb_2O_3. In the fabrication of nanostructures, EG is known to act in two ways: (1) a reducing agent as in the preparation of a series of metal or alloy nanoparticles [2a] and (2) a coordination agent (a temporary ligand) as in the preparation of SnO_2, TiO_2, PbO, and In_2O_3 nanoparticles [13]. We speculate that the chelating ligand EG binds strongly to antimony to form a more stable complex, whereas the nonchelating ligand EtOH weakly coordinates to the metal. The difference in coordinating capability between these two ligands seems to result in the selective preparation of the orthorhombic or cubic Sb_2O_3 phase. We also tried to prepare antimony compounds in glycerol–H_2O. However, no solid products were obtained, maybe because the tridentate ligand glycerol coordinates so strongly to the antimony metal to form a too stable compound that does not participate further in the subsequent reactions to give an ultimate product.

In order to confirm the effects of solvent composition on the phase of the final product, we performed the experiments in

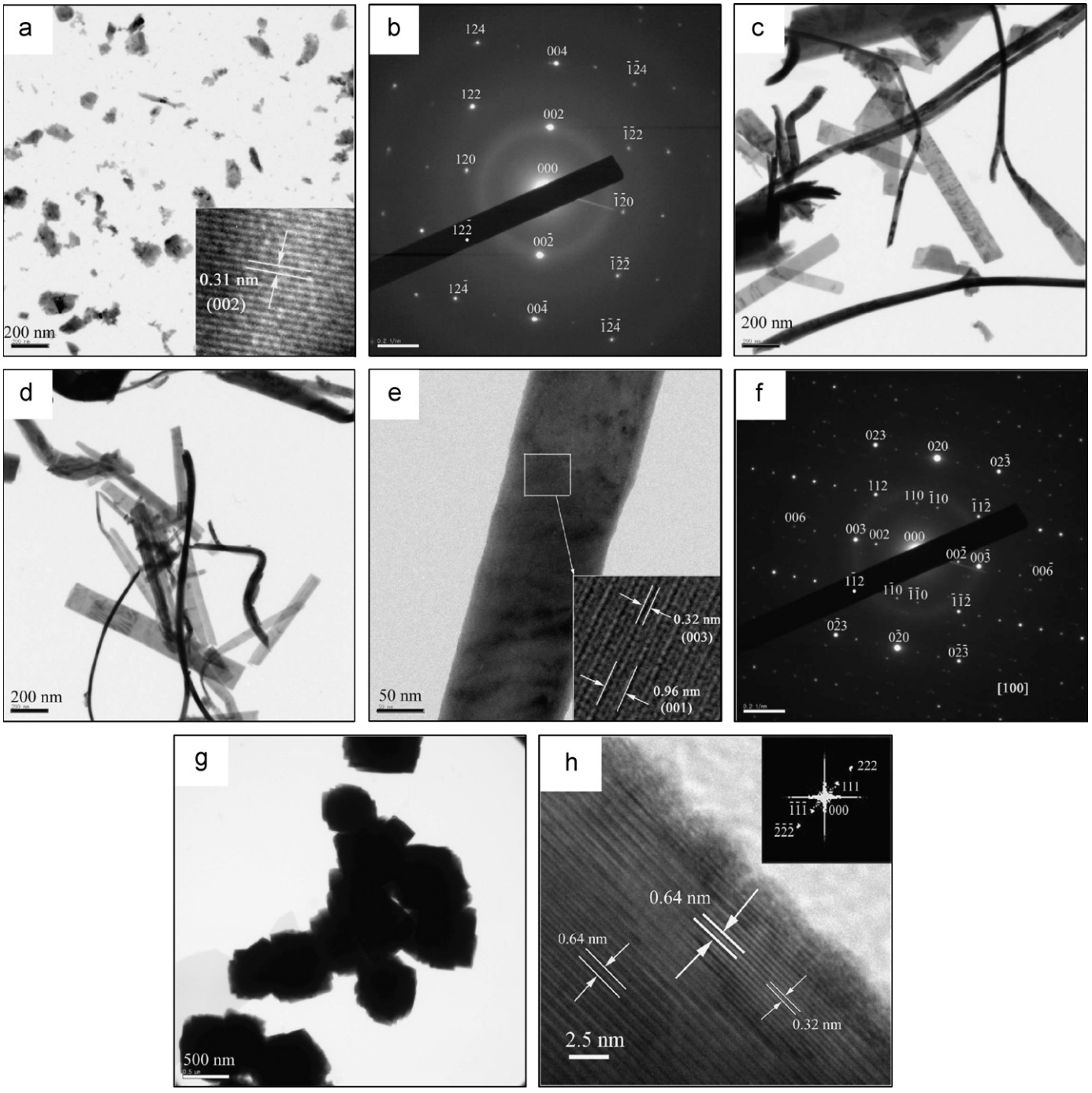

Fig. 4. TEM images of the samples prepared in EG–H_2O (v/v, 1:1): (a and b) $Sb_4O_5Cl_2$, (c–f) $Sb_8O_{11}Cl_2$, and (g and h) cubic Sb_2O_3.

several mixed solvents at constant acidity (pH = 8–9). As shown in Fig. 3, pure orthorhombic Sb_2O_3 could be obtained in dmf–H_2O (Fig. 3a) and toluene–H_2O (Fig. 3b). On the other hand, a mixture of orthorhombic Sb_2O_3 (major) and cubic Sb_2O_3 (minor) was formed in acetone–H_2O (Fig. 3c). Moreover, the cubic Sb_2O_3 was a sole product in en–H_2O (en = ethylenediamine; Fig. 3d). Consequently, the selective preparation of orthorhombic and cubic Sb_2O_3 can be achieved by selecting a proper solvent composition. It should be, however, mentioned that unlike dmf and acetone, toluene is basically immiscible with water, and therefore we are not sure whether the product is formed in organic phase (toluene) or in aqueous phase (H_2O).

Fig. 4 displays the TEM images of the samples obtained in EG–H_2O (v/v, 1:1) at 120 °C for 12 h at several pH ranges. The panoramic TEM image of the $Sb_4O_5Cl_2$ sample obtained at pH = 1–2 is shown in Fig. 4a, which illustrates the irregular nanoparticles in various sizes. The HRTEM image taken from one nanoparticle is presented in the inset of Fig. 4a, in which the lattice space of 0.31 nm corresponds to that of the (002) plane. In the case of $Sb_8O_{11}Cl_2$ obtained at pH = 4–5, its TEM images (Figs. 4c and d) show that the sample consists of nanobelts (major) and nanowires (minor) with the lengths up to several micrometers. Fig. 4e demonstrates the HRTEM image of a single $Sb_8O_{11}Cl_2$ nanowire, which has the typical lattice spaces of 0.32 and 0.96 nm corresponding to those of (003) and (001) planes. Furthermore, the SAED pattern in Fig. 4f illustrates that the 1-D $Sb_8O_{11}Cl_2$ nanowires grow preferentially in the [010] direction. However, at higher acidity (pH = 8–9), the cubic Sb_2O_3 was produced and it has the morphology of sub-micrometer particles (Fig. 4g). The corresponding HRTEM image obtained from the edge of the Sb_2O_3 particle is given in Fig. 4h, which shows the broad lattice spaces of 0.32 and 0.64 nm, consistent with those of the (222) and (111) planes.

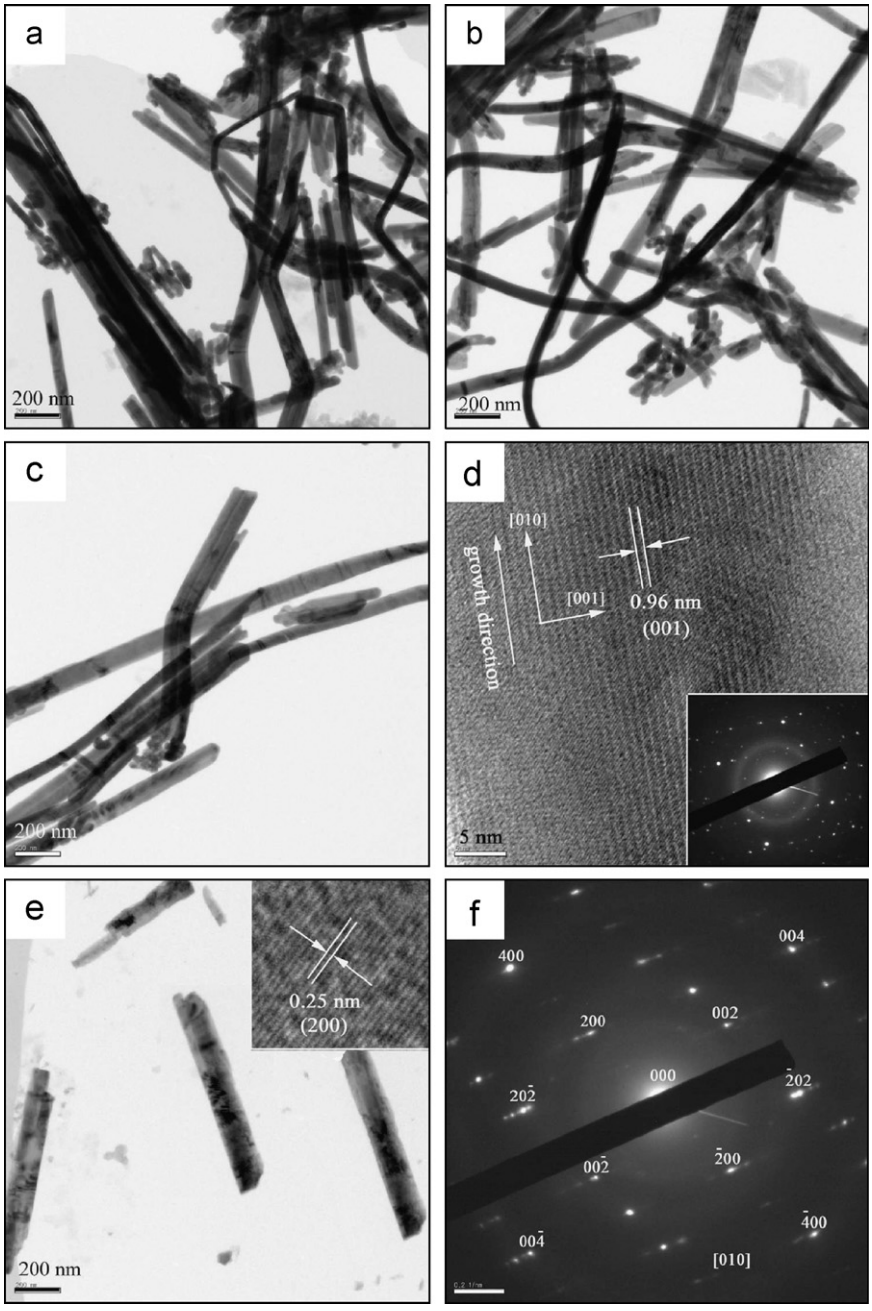

Fig. 5. TEM images of the samples prepared in EtOH–H_2O (v/v, 1:1): (a–d) $Sb_8O_{11}Cl_2$ and (e–f) orthorhombic Sb_2O_3.

Figs. 5a–c show the TEM images of $Sb_8O_{11}Cl_2$ synthesized at pH = 4–5 in EtOH–H_2O (v/v, 1:1), which demonstrate that the sample consists of many 1-D nanowires with an average diameter of 50 nm and lengths up to tens of micrometers. The corresponding HRTEM image of a single $Sb_8O_{11}Cl_2$ nanowire in Fig. 5d has the typical lattice space of 0.96 nm corresponding to that of the (001) plane. Based on the SAED pattern in the inset of Fig. 4d, we can figure out that the 1-D $Sb_8O_{11}Cl_2$ nanowires also grew preferentially in the [010] direction. It is worthwhile to note that the orthorhombic Sb_2O_3 sample prepared at pH = 8–9 has the morphology of 1-D nanorods with a relatively low aspect ratio (Fig. 5e), and that the cubic counterpart has the morphology of nanoparticles (Figs. 4g and h). The HRTEM image of the orthorhombic Sb_2O_3 (the inset of Fig. 5e) shows the lattice space to be about 0.25 nm, which corresponds to that of the (200) plane. In addition, these nanorods grew in the [001] direction, as shown in the SAED pattern in Fig. 5f.

Fig. 6 presents the TEM images of the orthorhombic Sb_2O_3 samples obtained at pH = 8–9 in toluene–H_2O (Fig. 6a) and en–H_2O (Fig. 6b). Whereas the reaction in toluene–H_2O gave tiny nanoparticles (Fig. 6a), the corresponding reaction in en–H_2O produced butterfly-like materials (Fig. 6b). In fact, the characteristics of the Sb_2O_3 sample formed in dmf–H_2O (not shown here) are practically the same as those in Fig. 6b. All phases and morphologies of the antimony oxychloride and oxide nanocrystals obtained at 120 °C for 12 h in mixed solvents are summarized in Table 2.

Figs. 1–6 tell us that the sizes, shapes, and phases of the antimony nanomaterials ($Sb_4O_5Cl_2$, $Sb_8O_{11}Cl_2$, and Sb_2O_3) in this study strongly depend on the acidity of a reaction mixture and composition of a mixed solvent. As mentioned above, the coordinating ability of a component in the mixed solvent appears to play an important role in determining the morphologies of the final products. For example, $Sb_4O_5Cl_2$ nanoparticles were formed in EG–H_2O, whereas micrometer $Sb_4O_5Cl_2$ crystals were formed in EtOH–H_2O. This difference in morphology may be due to the difference in growth rate of colloids, which are formed in the mixed solvent. The more strongly coordinating EG would slow down the growth of the colloids to give the $Sb_4O_5Cl_2$ nanoparticles. On the other hand, the weakly coordinating ethanol (EtOH) would let the colloids grow faster to develop the micrometer $Sb_4O_5Cl_2$ crystals.

Fig. 7 shows the room-temperature PL spectra of the Sb_2O_3 samples excited at 215 nm. The curve in Fig. 7a illustrates that the cubic Sb_2O_3 nanoparticles, which were prepared in EG–H_2O, have several emission bands: one sharp and strong band at 372 nm (3.33 eV) as well as three weak shoulders at 424 (2.92 eV), 486 (2.55 eV), and 534 nm (2.32 eV). Considering the band gap of bulk

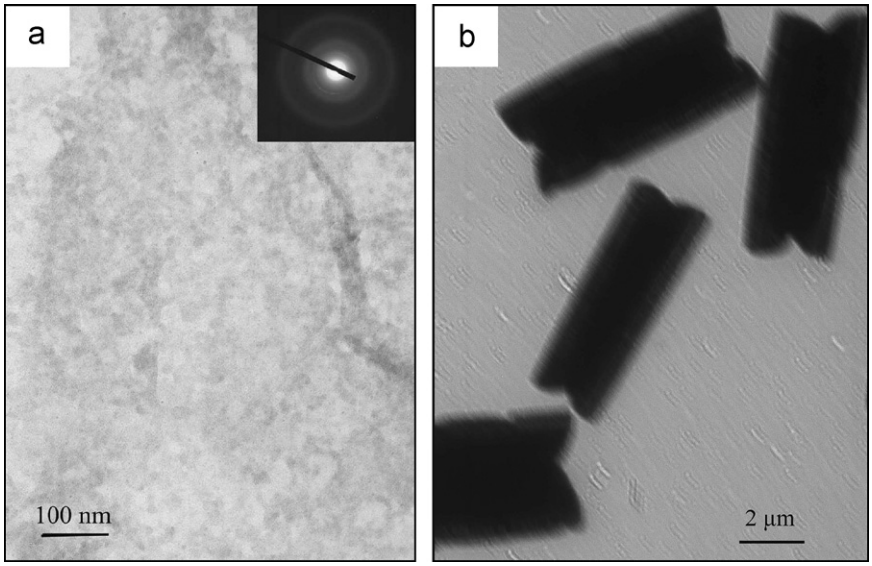

Fig. 6. TEM images of Sb_2O_3 samples obtained in mixed solvents (v/v, 1:1) at pH = 8–9: (a) toluene–H_2O and (b) en–H_2O.

Table 2
Summary of antimony oxychloride and oxide nanocrystals obtained at 120 °C for 12 h in mixed solvents

Product	pH	Mixed solvent (v/v: 1:1)	Phase	Morphology
$Sb_4O_5Cl_2$	1–2	EG–H_2O	Monoclinic	Nanoparticles
		EtOH–H_2O	Monoclinic	Irregular microcrystals
$Sb_8O_{11}Cl_2$	4–5	EG–H_2O	Monoclinic	Nanobelts[a] and nanowires[b]
		EtOH–H_2O	Monoclinic	Nanowires
Sb_2O_3	8–9	EG–H_2O	Cubic	Nanoparticles
		EtOH–H_2O	Orthorhombic	Nanorods
		dmf–H_2O	Orthorhombic	Microrods
		Toluene–H_2O	Orthorhombic	Nanoparticles
		Acetone–H_2O	Orthorhombic[a] and cubic[b]	Nanoparticles
		en–H_2O	Orthorhombic	Microrods

[a] Represents a major product.
[b] Represents a minor product.

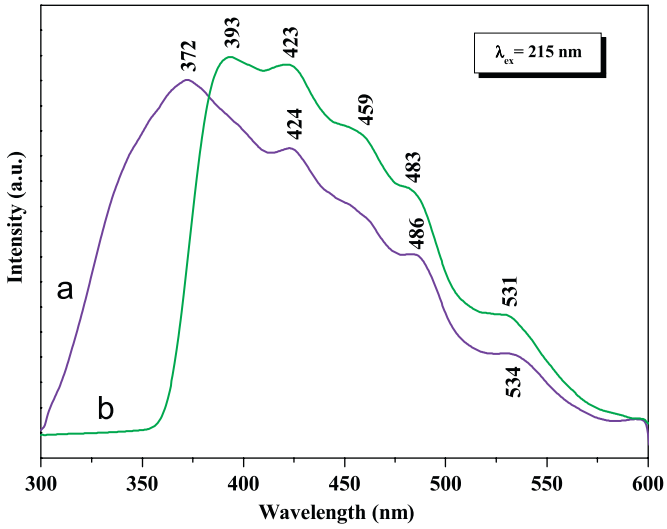

Fig. 7. Room-temperature PL spectra at $\lambda_{ex} = 215$ nm: (a) cubic Sb_2O_3 nanoparticles and (b) orthorhombic Sb_2O_3 nanorods.

senarmontite (4.31 eV) [14], the present cubic Sb_2O_3 sample exhibits a significant red shift. The corresponding PL spectrum of the orthorhombic counterpart (Fig. 7b) also displays several emission bands: one strong band at 393 nm (3.16 eV) and several weak shoulders at 423 (2.93 eV), 459 (2.70 eV), 483 (2.57 eV), and 531 nm (2.34 eV). The orthorhombic sample also exhibits a red shift, compared to bulk valentinite whose band gap is 3.30 eV [15]. Consequently, the present cubic and orthorhombic Sb_2O_3 both exhibit a red shift, which might be utilized in the field of optoelectronic devices [16].

4. Conclusions

In summary, a simple solution-phase approach was developed to prepare $Sb_4O_5Cl_2$, $Sb_8O_{11}Cl_2$, and Sb_2O_3 nanocrystals in various sizes, shapes, and phases. The acidity of a reaction mixture and composition of a mixed solvent were found to be the critical factors in preparing these nanocrystals. $Sb_4O_5Cl_2$, $Sb_8O_{11}Cl_2$, and Sb_2O_3 nanocrystals were prepared at pH = 1–2, 4–5, and 8–9, respectively. In particular, the EtOH–H_2O, dmf–H_2O, en–H_2O, and toluene–H_2O solvents were favored for the formation of the orthorhombic Sb_2O_3, whereas the EG–H_2O solvent was favored for the formation of the cubic Sb_2O_3. The PL spectra of the cubic and orthorhombic Sb_2O_3 samples exhibited a red shift compared to the corresponding bulk materials.

Acknowledgment

This work was supported by the Korea Research Foundation Grant funded by the Korean Government (MOEHRD) (KRF-2005-005-J11902).

References

[1] (a) J.T. Hu, T.W. Odom, C.M. Lieber, Acc. Chem. Res. 32 (1999) 425;
(b) Y.W. Jun, J.S. Choi, J.W. Cheon, Angew. Chem. Int. Ed. 45 (2006) 3414;
(c) C.N.R. Rao, F.L. Deepak, G. Gundiah, A. Govindaraj, Prog. Solid State Chem. 31 (2003) 5;
(d) H.C. Zeng, J. Mater. Chem. 16 (2006) 649.
[2] (a) Y.N. Xia, P.D. Yang, Y.G. Sun., Y.Y. Wu, B. Mayers, B. Gates, Y.D. Yin, F. Kim, H.Q. Yan, Adv. Mater. 15 (2003) 353;
(b) X. Wang, Y.D. Li, Inorg. Chem. 45 (2006) 7522;
(c) Z.W. Pan, Z.R. Dai, Z.L. Wang, Science 291 (2001) 1947.
[3] (a) A.E. Whitten, B. Dittrich, M.A. Spackman, P. Turner, T.C. Brown, Dalton Trans. (2004) 23;
(b) P.S. Gopalakrishnan, H. Manohar, J. Solid State Chem. 15 (1975) 61.
[4] R.D. Bernett, J. Mater. Sci. 39 (2004) 1075.
[5] J. Spengler, F. Anderle, E. Bosch, R.K. Grasselli, B. Pillep, P. Behrens, O.B. Lapina, A.A. Shubin, H.J. Eberle, H. Knözinger, J. Phys. Chem. B 105 (2001) 10772.
[6] K. Terashima, T. Hashimoto, T. Uchino, S.H. Kim, T. Yoko, J. Ceram. Soc. Japan 104 (1996) 1008.
[7] (a) L. Costa, P. Goberti, G. Paganetto, G. Camino, P. Sgarzi, Polym. Degrad. Stab. 30 (1990) 13;
(b) V.V. Bogdanova, S.S. Fedeev, A.I. Lesnikovich, I.A. Klimovtsova, V.V. Sviridov, Polym. Degrad. Stab. 11 (1985) 205.
[8] (a) X.Y. Chen, X. Wang, C.H. An, J.W. Liu, Y.T. Qian, Mater. Res. Bull. 40 (2005) 469;
(b) C.H. Ye, G.W. Meng, L.D. Zhang, G.Z. Wang, Y.H. Wang, Chem. Phys. Lett. 363 (2002) 34.
[9] Z.T. Deng, F.Q. Tang, D. Chen, X.W. Meng, L. Cao, B.S. Zou, J. Phys. Chem. B 110 (2006) 18225.
[10] (a) D. Sendor, T. Weirich, U. Simon, Chem. Commun. (2005) 5790;
(b) Y.X. Zhang, G.H. Li, J. Zhang, L.D. Zhang, Nanotechnology 15 (2004) 762.
[11] Z. Mayerová, M. Johnsson, S. Lidin, Solid State Sci. 8 (2006) 849.
[12] X. Su, Y. Liu, C. Xiao, G. Zhang, T. Liu, J.G. Qian, C.T. Chen, Mater. Lett. 60 (2006) 3879.
[13] (a) Y.L. Wang, X.C. Jiang, Y.N. Xia, J. Am. Chem. Soc. 125 (2003) 16176;
(b) R.W.J. Scott, N. Coombs, G.A. Ozin, J. Mater. Chem. 13 (2003) 969;
(c) J.Y. Kempf, B. Maigret, D.C. Crans, Inorg. Chem 35 (1996) 6485.
[14] A. Kyono, M. Kimata, M. Mastsuhisa, Y. Miyashita, K. Okamoto, Phys. Chem. Miner. 29 (2002) 254.
[15] N. Tigau, V. Ciupina, G. Prodan, G.I. Rusu, E. Vasile, J. Cryst. Growth 269 (2004) 392.
[16] Z.T. Deng, D. Chen, F.Q. Tang, X.W. Meng, J. Ren, L. Zhang, J. Phys. Chem. C 111 (2007) 5325.